International Journal of Pharmaceutics 674 (2025) 125480

Contents lists available at ScienceDirect

International Journal of Pharmaceutics

journal homepage: www.elsevier.com/locate/ijpharm

Dual-Loaded Chitosan-Based Nanoparticles: A Novel approach for treating polymicrobial osteomyelitis

M. Zegre [a,b], J. Barros [c,d], A.B. David [a], L. Fialho [c,d], M.P. Ferraz [c,d,e], FJ. Monteiro [c,d,e], L.A. Caetano [a,b], L. Gonçalves [a], A. Bettencourt [a,*]

[a] Research Institute for Medicines (iMed.ULisboa), Faculdade de Farmácia, Universidade de Lisboa, Av. Prof. Gama Pinto, 1649-003 Lisboa, Portugal
[b] H&TRC – Centro de Investigação em Saúde e Tecnologia, ESTeSL – Escola Superior de Tecnologia da Saúde de Lisboa, IPL – Instituto Politécnico de Lisboa, Av. D. João II, Lote 4.69.01, 1990-096 Lisboa, Portugal
[c] i3S – Instituto de Investigação e Inovação em Saúde – Associação, Universidade do Porto, R. Alfredo Allen 208, 4200-135 Porto, Portugal
[d] INEB – Instituto de Engenharia Biomédica, Universidade do Porto, R. Alfredo Allen 208, 4200-135 Porto, Portugal
[e] Departamento de Engenharia Mecânica, Faculdade de Engenharia, Universidade do Porto, s/n, R. Dr. Roberto Frias 4200-465, Portugal

ARTICLE INFO

Keywords:
Biofilm infections
Drug delivery system
Minocycline
Mixed osteomyelitis, polysaccharide nanoparticles
Voriconazole

Chemical compounds studied in this article:
Chitosan
Minocycline hydrochloride
Poloxamer
Voriconazole

ABSTRACT

Developing innovative approaches to target osteomyelitis caused by polymicrobial infections remains a significant therapeutic challenge. In this study, monodispersed chitosan nanoparticles co-loaded with antibacterial (minocycline) and antifungal (voriconazole) agents were successfully prepared. Minocycline presented higher encapsulation efficiency as compared to voriconazole. Thermostability analysis suggested interactions between the co-loaded drugs within the dual-delivery system, potentially limiting voriconazole release. The dual-loaded chitosan nanoparticles exhibited significant *in vitro* anti-biofilm activity, achieving up to a 90% reduction in polymicrobial biofilms of *S. aureus* and *C. albicans*. Additionally, the nanoparticles showed cytocompatibility with a human osteoblast cell line. These findings highlight the potential of this dual-delivery chitosan-based nanoparticle system to address a critical gap in osteomyelitis treatment by targeting both bacterial and fungal pathogens.

1. Introduction

Osteomyelitis is an acute or chronic inflammation of bone and its structures, caused by a microbial (*e.g.*, bacteria, fungi, and mycobacteria) infection, which leads to gradual bone destruction and loss (Bury et al., 2021; Dinh et al., 2009). A critical driver of osteomyelitis pathogenicity is biofilm formation – a community of sessile microorganisms embedded in a self-produced extracellular matrix. Biofilms significantly impair therapeutic efficacy and contribute to high rates of infection recurrence (Masters et al., 2022).

Approximately one-third of osteomyelitis cases are polymicrobial, with *Staphylococcus aureus* (the predominant pathogen) frequently coexisting with opportunistic fungi like *Candida albicans* (Enz et al., 2021; Gimza and Cassat, 2021; Hsu et al., 2023; Masters et al., 2022). Such mixed-species biofilms exacerbate infection severity by enhancing pathogen resistance to antimicrobial agents and immune responses, resulting in worsened clinical outcomes (Hsu et al., 2023; Masters et al., 2022). Consequently, osteomyelitis remains a challenging condition to treat, associated with high morbidity and substantial healthcare costs (Masters et al., 2022; Schmidt et al., 2023). Understanding the interplay between co-infecting pathogens and biofilm dynamics is crucial to advancing therapeutic strategies for this debilitating condition (Zegre et al., 2022).

Current treatment strategies for osteomyelitis, such as prolonged systemic antibiotic administration combined with surgical debridement, often fail to fully eradicate biofilms, highlighting the urgent need for alternative approaches (Tao et al., 2021). Among emergent strategies, nanotechnology has garnered significant interest in osteomyelitis treatment due to nanomaterials capability to overcome biological barriers, enhance drug bioavailability, and enable controlled release. In light of this, chitosan-based nanoparticles (NPs) are particularly attractive for osteomyelitis treatment due to their antimicrobial activity,

* Corresponding author at: Research Institute for Medicines (iMed.ULisboa), Faculdade de Farmácia, Universidade de Lisboa, Avenida Prof. Gama Pinto, 1649-003 Lisboa Portugal.
E-mail address: asimao@ff.ulisboa.pt (A. Bettencourt).

https://doi.org/10.1016/j.ijpharm.2025.125480
Received 6 January 2025; Received in revised form 13 March 2025; Accepted 14 March 2025
Available online 15 March 2025

bioadhesive properties, and biocompatibility. These NPs facilitate the encapsulation and delivery of both hydrophilic and hydrophobic drugs, enhancing their stability, bioavailability, and therapeutic efficacy, (Zapata et al., 2022), (Mikušová and Mikuš, 2021; Shi et al., 2024). Several methods have been reported for preparing chitosan NPs including ionic gelation, emulsification, crosslinking, complexation with polyelectrolytes, self-assembly, and drying processes (Mikušová and Mikuš, 2021). Additionally, the inclusion of surfactants such as poloxamer 188 (Pluronic® F68) or polysorbate 80 (tween® 80) plays a crucial role in stabilizing nanoparticle formulations. These surfactants present low toxicity and are used to stabilize particle size, drug load, and release profiles while avoiding nanoparticle agglomeration (Mikušová and Mikuš, 2021; Miyazawa et al., 2021; Rasyid et al., 2014).

Moreover, the efficacy of antibiotic-loaded NPs in treating osteomyelitis has been proved in numerous studies (Ma et al., 2016; Mohan Raj et al., 2022; Simpson et al., 2024; Tao et al., 2020). Among the used antibiotics, tetracyclines – particularly minocycline – have proven to be effective due to their broad-spectrum activity and ability to target multi-resistant bacteria (Martin et al., 2024). Minocycline, in particular, exhibits significant *in vitro* activity against *Staphylococcus aureus*, including methicillin-resistant strains, making it a strong candidate for osteomyelitis therapy (Im et al., 2020; Martin et al., 2024; Silva et al., 2017; Wen et al., 2024). On the other hand, studies focusing on antifungal-loaded carrier systems for fungal osteomyelitis are limited, and none have explored the potential of nanomaterials in this context (Grimsrud et al., 2011; Karr and Lauretta, 2015). While antibiotic-loaded chitosan NPs have shown efficacy in treating bacterial osteomyelitis, the development of dual-delivery systems targeting both bacterial and fungal pathogens is still in its infancy (AbouAitah et al., 2022).

Addressing these gaps, the present study aimed at developing and evaluating mono- and dual-delivery systems using chitosan NPs stabilized with Pluronic® F68, loaded with minocycline and voriconazole. We hypothesize that dual-loaded chitosan-based NPs could effectively treat polymicrobial osteomyelitis by acting as a polysaccharide-based carrier to enhance antimicrobial delivery, improve biofilm penetration, and facilitate comprehensive infection management.

2. Materials and methods

2.1. Reagents

Low molecular weight chitosan (50 to 100 kDa, 92,2% deacetylated) and 3-(4,5-dimethyl-2-thiazolyl)-2,5-diphenyl-2H-tetrazolium bromide (MTT) were obtained from Sigma-Aldrich (Irvine, UK). Sodium tripolyphosphate (TPP) was acquired from Applichem (Darmstadt, DE). Minocycline hydrochloride was kindly donated by Atral Cipan (Castanheira do Ribatejo, PT) and voriconazole was obtained from Glentham Life Sciences (Corsham, UK). Pluronic ® F68 was acquired from BASF (Ludwigshafen, DE). HEPES buffer was purchased from VWR Chemicals (USA). Propidium iodide was granted by Invitrogen Thermo Fisher Scientific (San Francisco, USA) and dimethylsulfoxide (DMSO) was obtained from Sigma-Aldrich (USA).

Tryptic Soy Broth (TSB), Tryptic Soy Agar (TSA) Sabouraud Dextrose Agar (SDA), and NaCl were purchased from Merck Millipore (Germany), while the Mannitol Salt Agar (MSA) was acquired from Liofilchem (Italy).

All other reagents and solvents were of the purest grade available and used without further treatment. Purified water (Millipore, Elix 3) was filtered using a 0.20 μm membrane filter.

2.2. Preparation of chitosan nanoparticles

Chitosan was mixed with 1 % v/v acetic acid to a final concentration of 10 mg/mL and at pH 5.5. Drug loading on chitosan NPs was done by adding 1 mg/mL minocycline (100 μL) and/or 2.5 mg/mL voriconazole in DMSO (10 μL) to the chitosan solution. Then, 10 mg/mL TPP (50 μL) and variable volumes (150 μL, 50 μL, 140 μL and 40 μL, to b-NPs, Min-NPs, Vor-NPs and Min-Vor-NPs, respectively) of 0.1 % Pluronic® F68 was added to the chitosan solution and homogenized by pipetting, to a final 2 mg/mL chitosan concentration. In the end, four batches of chitosan NPs were prepared (in triplicate): minocycline-loaded NPs (Min-NPs), voriconazole-loaded NPs (Vor-NPs), minocycline-and-voriconazole-loaded NPs (Min-Vor-NPs), and unloaded or blank NPs (b-NPs) (used as control). The prepared batches of NPs were frozen for 1 h, before being freeze-dried (Christ Alfa 1–4, Germany) for at least 2 h.

2.3. Physicochemical characterization of chitosan nanoparticles

2.3.1. Particle size and zeta potential

Mean particle size and polydispersity index (PI) were determined by dynamic light scattering with a Zetasizer Nano-S (Malvern Instruments, Worcestershire, UK) at a detection angle of 175° and a temperature of 25 °C with 2 min of stabilization time before measurements. The samples were dispersed in purified filtered water (refraction index 1.330; viscosity 0.8872 cP, 25 °C). Each sample was measured in triplicates.

Zeta potential was measured by electrophoresis mobility using a Zetasizer Nano-Z (Malvern Instruments, Worcestershire, UK). Samples were diluted with 0.45 μm filtered ultra-pure water. For all cases, mean values were obtained from the analysis of three different batches, each measured in triplicates.

2.3.2. Fourier transform infrared spectroscopy (FTIR)

Attenuated total reflection-Fourier transform infrared (ATR-FTIR) spectra of the chitosan, free drugs, and drug-loaded chitosan nanoparticles (NPs) were obtained with an ATR-FTIR spectrometer (Platinum-ATR Brucker spectrometer) to characterize the chemical structure of chitosan NPs. The spectra were scanned over the wave number range of 400 to 4000 cm^{-1}, with an average of 24 scans and a resolution of 2 cm^{-1}.

2.3.3. Differential scanning calorimetry (DSC)

The thermal behavior of chitosan NPs was studied using DSC analysis in a DSCQ200 (TA Instruments, New Castle, DE, USA); freeze-dried samples (1–2 mg) were sealed on a standard aluminum pan, and heated from 0 °C to 300 °C at a scan rate of 10 °C/minutes under a nitrogen atmosphere. An empty sealed pan was used as reference.

2.4. Drug loading and entrapment efficiency

The percentage of drug loading (DL%) and entrapment efficiency (EE %) were indirectly determined by measuring the concentration of the free drug present in the supernatant obtained by centrifugation (MiniSpin, Eppendorf, Hamburg, Germany) at 13,400 rpm for 5 min of the drug-loaded chitosan NPs. Minocycline quantification was established spectrophotometrically at 350 nm in a microplate reader (FLUOstar Omega, BMG Labtech, Germany) (Martin et al., 2019). Voriconazole quantification required chitosan precipitation, achieved by treating each sample with 10 % of NaOH (1.0 M), the samples were then centrifuged for 5 min (at 13,500 rpm), and voriconazole was quantified in the supernatant using a reversed-phase high-performance liquid chromatography (RP-HPLC) method. The analysis was performed on a Shimadzu System (Shimadzu Corporation, LC-6A, Japan) coupled to an autosampler (Waters 717plus Autosampler) and a thermostatic column compartment (Dionex STH 585 Column Oven). A LiChrospher® 100 RP-18 analytical column (125 mm × 4 mm, 5 μm particle size, LiChroCART®Merck, Darmstadt, Germany) was used at 30 °C. Isocratic elution was carried out with a mobile phase of acetonitrile–water (3:2), with flow rate of 1 mL/min. Detection was set at 256 nm and the injection volume was 20 μL (Babu and Raju, 2007; Üstündağ Okur et al., 2016; Zegre et al., 2022). Each experiment was performed in triplicate and the average values were calculated.

Free drug concentration was calculated by linear regression and %EE

and %DL were obtained through Equations (1) and (2), respectively, where $[C]_{total}$ corresponds to the total amount of minocycline and/or voriconazole initially loaded in the NPs, $[C]_{sup}$ is the measured concentration of minocycline and/or voriconazole in the supernatant, V_{total} is the total volume of each sample, and m_{total} is the mass of NPs in the samples.

$$\%EE = \frac{[C]_{total} - [C]_{sup}}{[C]_{total}} \times 100 \quad (1)$$

$$\%DL = \frac{([C]_{total} - [C]_{sup}) x V_{total}}{m_{total}} \times 100 \quad (2)$$

2.5. Drug release assay

Release studies were carried out by adding 1 mL of 10 mM HEPES buffer at pH 7.4 to each freeze-dried nanoparticle samples. The samples were then incubated at 37 °C with constant agitation. At various time-intervals, the samples were collected and centrifuged (Allegra™ 64R Centrifuge, Beckman Coulter, California, USA) at 13,000x g for 10 min, after which the supernatants were removed. Cumulative drug release quantification was measured in triplicate, using a microplate reader (for empty NPs and minocycline-loaded NPs) or RP-HPLC (for voriconazole-loaded NPs), according to the methodology previously described (2.4.). After removing and exchanging the supernatants, the samples were then resuspended in 1 mL HEPES and incubated again at 37 °C.

2.6. Antimicrobial activity

2.6.1. Microbial growth and standardization

The *S. aureus* ATCC 49230 strain was acquired from the ATCC supplier, and the *C. albicans* NQ6159 strain was gently donated by "Instituto Nacional de Saúde Doutor Ricardo Jorge (Portugal)". TSA medium was used to quantify mono-species *S. aureus* and dual-species *S. aureus-C. albicans;* MSA medium was used to quantify *S. aureus* selectively into dual-species biofilm, and SDA medium was used to quantify *C. albicans* into mono- and dual-species biofilms. Before each experiment, microorganisms were grown in TSB for 24 h at 37 °C and 150 rpm. After incubation, each microorganism's initial suspension (at exponential phase) of 1×10^6 CFU mL^{-1} was produced in fresh TSB and used in subsequent sections.

2.6.2. Anti-biofilm activity of chitosan nanoparticles over time

The anti-biofilm activity of the NPs (b-NPs, Min-NPs, Vor-NPs, and Min-Vor-NPs) against mono- and dual-species biofilm formation was evaluated following the protocol performed by (Zegre et al., 2022), with some modifications. For mono-species biofilms, 100 μL of *S. aureus* or *C. albicans* at 1×10^6 CFU mL^{-1} was added to 96-well tissue culture plates (TCP) while for dual-species *S. aureus–C. albicans* biofilms, 50 μL of each culture with an initial concentration of 2×10^6 CFU mL^{-1} was used. The TCP was incubated for 2 h at 37 °C and 120 rpm to induce pre-biofilm formation. Following incubation, the wells were carefully rinsed twice with 0.9 % NaCl, to remove planktonic and weakly attached cells. Then, 100 μL of NPs and fresh TSB medium (without microorganisms, 1:1 ratio) were added to pre-washed well-adhered biofilms. The plates were incubated for 2 and 24 h at 37 °C and 120 rpm, to form the mono- and dual-species biofilms. After each incubation time, the sessile microorganisms were rinsed twice with 0.9 % NaCl. Then, 100 μL of PBS was added to each well, and the TCPs were sonicated for 10 min using an ultrasonic water bath (BactoSonic Ultrasonic Bath BS14, 200 W, 40 kHz, Bandelin), to dislodge sessile microorganisms. The sessile populations were quantified through the Colony-Forming Units (CFUs) method. *S. aureus*, *C. albicans,* and *S. aureus-C. albicans* suspensions (free-NPs, free-antimicrobial agents, positive control 1), b-NPs (positive control 2) were used as positive controls, and minocycline (10 μg/mL, negative control 1), voriconazole (15 μg/mL, negative control 2), and minocycline-voriconazole (10 μg/mL-30 μg/mL negative control 3) solutions were used as negative controls.

2.7. Cytocompatibility assays

Cytocompatibility evaluation was conducted on all the studied groups of NPs, at two concentrations of 850 μg/mL and 425 μg/mL, using a human osteoblast-like cell line (MG-63, ATCC®CRL-1427™). Cells were expanded in RPMI 60 culture medium, containing 10 % fetal bovine serum (FBS), 100 IU/mL of penicillin G (sodium salt), 100 units/mL of streptomycin sulfate and 2 mM L-glutamine (all Gibco), at 37 °C and 5 % CO_2. At adequate confluence (70–80 %), grown cells were detached and inoculate in 96 well microplate at a cell density of 20,000 cells/well. Next day, the culture medium was removed, and cultures were incubated with a complete culture medium with different nanoparticle groups. Cells in culture media were used as negative control and sodium dodecyl sulfate (SDS) at 1 mg/mL as positive control. Cultures were characterized for membrane integrity and metabolic activity (Bettencourt et al., 2021).

2.7.1. Membrane integrity

Cell membrane integrity was assessed by propidium iodide (PI) uptake. After 24 h of incubation with the NPs, the medium was replaced with a 0.3 μM PI solution in culture medium and incubated for 15 min. Cells incubated only with the culture medium were used as a control. Fluorescence was measured (excitation: 485 nm; emission: 590 nm) in the microplate reader (FLUOstar Omega, BMGLabtech, Ortenberg, Germany). The propidium iodide uptake ratio from the cells was determined using Equation (3):

$$\text{Propidium iodide uptake ratio} = \frac{[Fluorescence]sample}{[Fluorescence]control} \quad (3)$$

2.7.2. Metabolic activity

The assessment of the cultures metabolic activity of the cultures was determined by the MTT assay. After 24 h of incubation with the NPs, the medium was replaced by a culture medium containing MTT (5 mg/mL) and incubated for 3 h. Then, the complete media was removed, and the intracellular formazan crystals were solubilized and extracted with 100 μL of dimethylsulfoxide (DMSO). The absorbance was measured at 570 nm with a microplate reader (FLUOstar Omega, BMGLabtech, Germany) (Bettencourt et al., 2021), and the relative cell viability determined (Equation (4).

$$\text{Cell viability} = \frac{[Absorbance]sample}{[Absorbance]control} x100 \quad (4)$$

2.8. Statistical data analysis

Quantitative data was presented as mean ± standard error. Data normality was evaluated using the Levene test. For normal data sets, one-way ANOVA was performed, followed by multiple comparisons using Tukey's test. The Kruskal-Wallis test was performed for non-parametric data sets, followed by multiple comparisons using Dunn's tests. p values ≤ 0.05 were considered significant. GraphPad Prism 8.0.1 (GraphPad Software, Boston, Massachusetts USA) was used as analysis software.

3. Results and discussion

Chitosan NPs, categorized into four groups (b-NPs, Min-NPs, Vor-NPs, and Min-Vor-NPs), were successfully produced in one single step by an ionotropic gelation method, as previously reported (Bettencourt al., 2021). Poloxamer Pluronic® F68 was selected as a stabilizing nonionic surfactant during nanoparticle formulation due to its well-known ability to improve the colloidal stability of the nanocarriers (Rasyid et al.,

2014). Additionally, the hydrophilic-lipophilic value (29) of Pluronic® F68 was considered crucial for its solubilization in the aqueous medium used for nanoparticle synthesis (Bernela et al., 2014).

3.1. Physical chemical characterization

3.1.1. Size and zeta analysis

Dynamic light scattering revealed that the chitosan NPs were monodispersed with low polydispersity index (PI) values (Table 1), indicating colloidal uniformity and minimized aggregation immediately after synthesis. The size distribution of chitosan NPs is affected by chitosan molecular weight as well as by the production method used. Previous studies on the production of chitosan NPs by ionotropic gelation with TPP found that the size distribution of the NPs ranged from 300 to 750 nm (Ha et al., 2019) or between 168 and 682 nm (Agarwal et al., 2018). Drug-loaded chitosan NPs exhibited slightly lower PI values than b-NPs. This effect was previously reported (Azevedo et al., 2014) suggesting that drug-loaded nanocarriers exhibit a more homogeneous size distribution. Among drug-loaded NPs, Min-NPs exhibited the smallest size (320.6 ± 5.7 nm), suggesting higher packing efficiency, which may result from void filling by minocycline in the nanoparticle matrix, leading to a more tightly packed structural arrangement. The smaller size of NPs improves drug delivery, as they are easier to transfer through biological membranes, and offers the potential to encapsulate more drugs, increase drug stability and absorption, and allow longer administration times (Warsito and Agustiani, 2021).

The hypothesis of better packing efficiency as a potential factor influencing nanoparticle size reduction is supported by experimental work (Kim et al., 2020). The interaction of Van der Waals forces and hydrogen bonding between minocycline and chitosan may contribute to reducing the size of minocycline-loaded NPs (Azevedo et al., 2014), as chitosan has a large content of hydroxyl and free amino groups, while minocycline contains oxygen and nitrogen components capable of participating in hydrogen bonding (Yazdanbakhsh et al., 2023). The size distribution of b-NPs (529.4 ± 32.0 nm) and Vor-NPs (518.9 ± 26.0 nm) was similar, and Min-Vor-NPs had an intermediate size range (466.8 ± 13.9 nm) between b-NPs and Min-NPs. This suggests that voriconazole to some extent decreases the packaging efficiency in chitosan NPs.

As expected, the zeta potential measurements showed that all NPs were positively charged (Table 1), due to the presence of residual protonated amine groups, since chitosan is a cationic polysaccharide (Aibani et al., 2021). The drug-loaded NPs presented a slightly higher ζ-potential than b-NPs (Table 1), indicating that drug loading contributed to greater particles stability, which makes them good candidates for single and dual drug delivery. We must note that the suitable NPs size and zeta potential observed after synthesis must be confirmed in future studies to ensure sufficient knowledge on their stability during storage, manipulation and in vivo applications (Kamiya et al., 2022; Phan and Haes, 2019).

3.1.2. Chemical and thermal analysis

The ATR-FTIR spectra of chitosan, minocycline, voriconazole, chitosan NPs, and drug-loaded chitosan NPs are depicted in Fig. 1a. Minocycline (dark blue spectrum) sharped peak at 3478 cm^{-1} indicate O–H and N–H stretching vibrations ((Rodrigues et al., 2014)); the absorption peaks at 1470 and 1042 cm^{-1} indicate structural vibrations of benzene rings and C-O stretching vibrations, respectively (Janakiraman et al., 2020); the absorption band at 1523 cm^{-1} indicates N–H bending (Reddy et al., 2014). Other distinctive peaks were detected at 1582, 1402, 828, 673, and 574 cm^{-1} (Rodrigues et al., 2014). Voriconazole (light blue spectrum) peaks at 1586, 1278, 1128, and 778 and cm^{-1} indicate C–C aromatic stretching, C-N stretching, C-O stretching, and aromatic banding vibration, respectively (Füredi et al., 2017). Other bands indicate O–H stretching at 3201–3047 cm^{-1}, C-F stretching at 1586–1452 cm^{-1} and C-N stretching at 1510–1452 cm^{-1} (Bhosale et al., 2016). Chitosan (red spectrum) peaks at 1644 cm^{-1}, 1569 $cm^{-1,}$ and 1320 cm^{-1}, correspond to C=O stretching (amine I), N–H bending (amine II), and C-N stretching (amine III). C-O stretching corresponds to bands at 1066 and 1028 cm^{-1}. The 896 cm^{-1} band indicates the C–H bending out of the plane of the ring of monosaccharides (Fernandes Queiroz et al., 2014).

The characteristic chitosan peaks were confirmed in all NPs spectra, whereas drug peaks were mostly absent. In drug-loaded chitosan NPs (Vor-NPs – pink spectrum; Min-NPs – purple spectrum; Min-Vor-NPs – light yellow spectrum), and in blank NPs (b-NPs – orange spectrum) characteristic chitosan peaks were observed at 3347 cm^{-1}, 2883 cm^{-1}, 1657 cm^{-1}, and 1598 cm^{-1}. The results suggest that there are no chemical interactions between the drugs and the polymer since voriconazole and minocycline did not significantly alter the chemical composition of chitosan NPs. These findings are also consistent with the low drug loading values obtained (Table 2), and with chitosan's high chemical stability (Karakeçili et al., 2019), determined by its molecular structure, making it a very versatile biomaterial for biomedical applications (Abinaya et al., 2019).

Differential scanning calorimetry (DSC) was used to investigate the effect of drug loading on the thermal properties of the synthesized NPs (Fig. 1b) (Matos et al., 2014). Minocycline, voriconazole, Pluronic® F68 and chitosan were used as controls.

From chitosan thermogram analysis, the reported endothermic peak around 79 °C – also called dehydration temperature (Chandra Dey et al., 2016) – was not observed, indicating the thermal behavior of essentially dry chitosan. The main feature was a sharp melting endothermic peak at 182 °C, which may be due to the process of dissociation of interchain hydrogen bonding of the polymer, which is strongly formed among the –OH and $–NH_2$ functional groups (El-Hafian et al., 2010). From the voriconazole DSC curve, a sharp endothermic peak can be recognized at 131 °C as described elsewhere (Mohan and Gupta, 2019). From minocycline thermogram analysis, two endothermic peaks may be found at 193 °C and 215 °C – similar peaks have been described at 187 °C, 197 °C (Rodrigues et al., 2014)) and 219 °C (Siddiqui et al., 2022). For all these three substances (chitosan, voriconazole and minocycline) no glass transition was detected, establishing that they were all essentially in the crystalline phase, once this phenomenon occurs when amorphous material is cooled or heated in a specific temperature range (Ghosh Dastidar and Chakrabarti, 2019).

Regarding the NPs formulations, as the chitosan endothermic peak (around 182 °C) is absent in all the NPs formulations, it may be hypothesized that chitosan is typically in an amorphous phase in the nanocarriers. The Pluronic® F68 peak (around 46 °C in pure form) was observed with slight deviations in all NP groups, as follows: 42 °C in Vor-NPs, 41 °C in Min-NPs, 43 °C in Min-Vor-NPs, and 45 °C in b-NPs (being absent in free drugs and physical mixtures). The voriconazole peak is found in the Vor-NPs but at 214 °C, while the minocycline peak is also observed at a different temperature (120 °C), as shifts of endothermic and exothermic peaks are commonly associated with interactions between polymer and drugs (Mori et al., 2017; Sarmento et al., 2006). The identified endothermic peaks associated with the drugs in single delivery formulations were not recognized in Min-Vor-NPs, indicating that both drugs should be in an amorphous phase in this arrangement, a property that can influence drug release from the NPs (Dinarvand et al., 2012), although this further confirms that minocycline and voriconazole are encapsulated in the formulation (Siddiqui et al., 2022).

Table 1
Physicochemical characterization of chitosan NPs, encompassing the particle size, polydispersity index (PI) and zeta potential. Mean ± SD (n = 3).

Formulation	Particle size (nm)	PI	Zeta potential (mV)
b-NPs	529.4 ± 32.0	0.679 ± 0.1	+33 ± 0.9
Min-NPs	320.6 ± 5.7	0.415 ± 0.0	+39 ± 1.6
Vor-NPs	518.9 ± 26.0	0.596 ± 0.1	+37 ± 0.4
Min-Vor-NPs	466.8 ± 13.9	0.504 ± 0.0	+41 ± 1.2

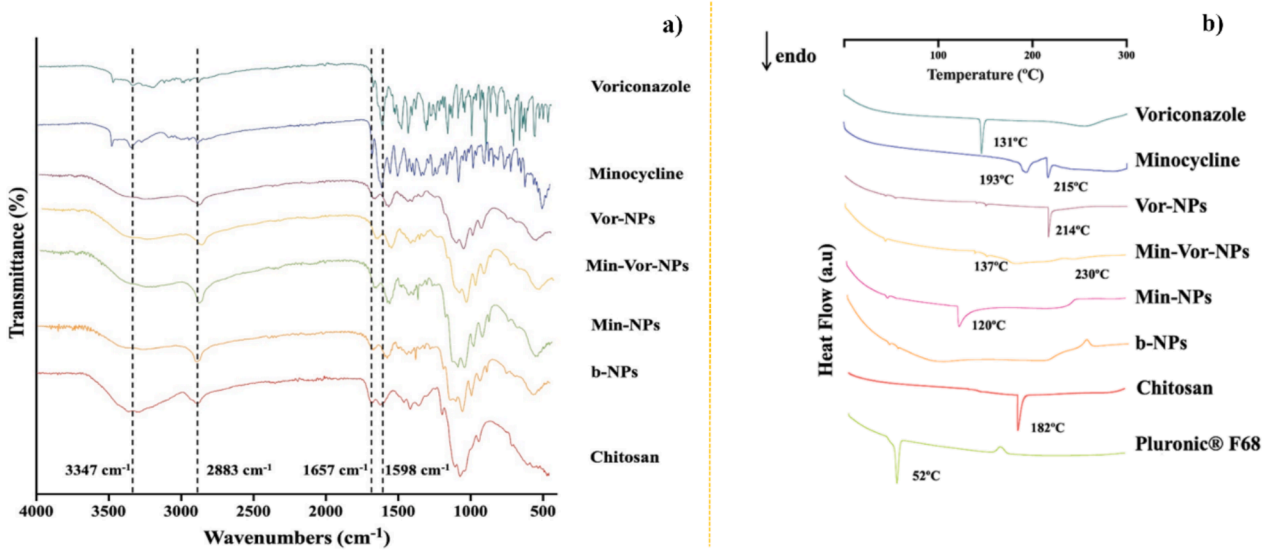

Fig. 1. Physicochemical characterization of chitosan NPs. (a) ATR-FTIR spectra of voriconazole, minocycline, chitosan, voriconazole-loaded chitosan NPs (Vor-NPs), minocycline-loaded chitosan NPs (Min-NPs), voriconazole- and minocycline-loaded chitosan NPs (Min-Vor-NPs), and blank chitosan NPs (b-NPs). (b) Thermograms obtained from blank (b-NPs) and drug-loaded NPs, free drugs (minocycline, voriconazole), chitosan and Pluronic® F68. Mean ± SD (n = 3).

Table 2
Entrapment efficiency (EE) and drug loading (DL) percentages of chitosan NPs. Mean ± SD (n = 3).

Formulation		EE (%)	DL (%)
b-NPs		–	–
Min-NPs		9.07 ± 2.50	0.50 ± 0.13
Vor-NPs		57.47 ± 1.76	1.03 ± 0.03
Min-Vor NPs	Minocycline	6.97 ± 2.67	0.37 ± 0.13
	Voriconazole	53.40 ± 1.93	0.97 ± 0.03

3.2. Entrapment efficiency and drug loading

Entrapment efficiency (%EE) indicates the percentage of the encapsulated drug in the NPs compared to the total active substance added (Rabima and Sari, 2019). As shown in Table 2, both drugs were successfully entrapped by the chitosan NPs. A relatively high amount of voriconazole was loaded onto single- and dual-drugs NPs, with EE of voriconazole above 50 % (57.47 ± 1.76 % for Vor-NPs; 53.40 ± 1.93 % for Min-Vor-NPs). These %EE results agree with previous studies on chitosan NPs loaded with voriconazole, in which it was observed that the presence of surfactants improved the %EE within a similar range (Shah et al., 2021). On the contrary, %EE of minocycline was below 10 % (9.07 ± 2.50 % for Min-NPs; 6.97 ± 2.67 % for Min-Vor-NPs).

The different %EE values observed can be attributed to different drug solubilities. Voriconazole is a hydrophobic drug with low water solubility (98 μg/mL) (de Almeida Campos et al., 2023), whereas minocycline hydrochloride is water-soluble (16 mg/mL at 25 °C) (Zbinovsky and Chrekian, 1977). Minocycline frequently exhibits poor encapsulation efficiencies in polymeric biodegradable NPs, due to its solubility in aqueous solutions (Holmkvist et al., 2016). Although chitosan NPs can incorporate both water-soluble and insoluble drugs (Jafernik et al., 2023), chitosan often behaves as a hydrophobic polymer (Yanat and Schroën, 2021). Surfactants such as Pluronic® F68, decrease the surface tension of the polymer solution, resulting in a more flexible droplet formation, hence, in a higher percentage of drug entrapped. High entrapment efficiency can also be obtained if no drug leakage occurs from the matrix during formulation preparation. In order to encapsulate slightly water-soluble drugs, maintaining a low temperature during the formulation process can help to reduce drug water-solubility and avoid drug partitioning into the aqueous phase. Differences may also be due to different drugs concentrations during NPs preparation: 83.33 μg/mL for minocycline *vs.* 20.83 μg/mL for voriconazole.

Drug loading (%DL) is another key parameter to characterize NPs, being defined as the mass ratio of drug to drug-loaded nanocarriers. It depends on several factors related to the drug, excipients, and preparation method. By containing a high drug load, high-dose pharmaceutical formulations improve the drug/excipient ratio, improving the biocompatibility profile. Currently, most NPs display DL values below 10 %, making it necessary to develop methods to increase drug loading (Liu et al., 2020). Thus, the obtained low values of %DL for both drugs (Table 2) were as expected.

3.3. In vitro drug release

In vitro drug release profiles are shown in Fig. 2. Min-NPs (Fig. 2a) showed an initial burst release of minocycline at 2 h (60.7 ± 1.5 %; 10.93 ± 2.03 μg/mL) followed by constant release after 4 h until maximum cumulative release at 28 h (73.9 ± 11.6 %), similarly to results (77.46 ± 1.17 %) reported elsewhere (Nagpal et al., 2013). In Min-Vor-NPs (Fig. 2c), a burst release of minocycline in the first 2 h (99.5 ± 0.20 %; 17.9 ± 0.69 μg/mL) was also observed, with maximum cumulative release at 24 h (101.7 ± 3.80 %; 18.3 ± 0.69 μg/mL). The higher maximum cumulative release of minocycline in Min-Vor-NPs suggest differences in drug packaging in the polymer matrix in the presence of voriconazole (probably due to some competitive chemical interactions), promoting minocycline's total release.

In vitro drug release was lower in Vor-NPs (Fig. 2b), with burst release at 2 h (27.7 ± 0.40 %; 5.5 ± 1.51 μg/mL) followed by constant release until 24 h (27.7 ± 0.50 %; 5.5 ± 1.50 μg/mL). It was not possible to quantify voriconazole release from Min-Vor-NPs, which may be related to the findings from DSC analysis, where the antifungal was identified in the amorphous phase.

Drug solubilities strongly influence drug distribution in the polymeric matrix and, consequently, the extent of drug release by NPs, which impacts drug bioavailability (Kalepu and Nekkanti, 2015). The phenomena involved in drug release from chitosan NPs include polymer swelling, drug diffusion through the polymeric medium, diffusion of the

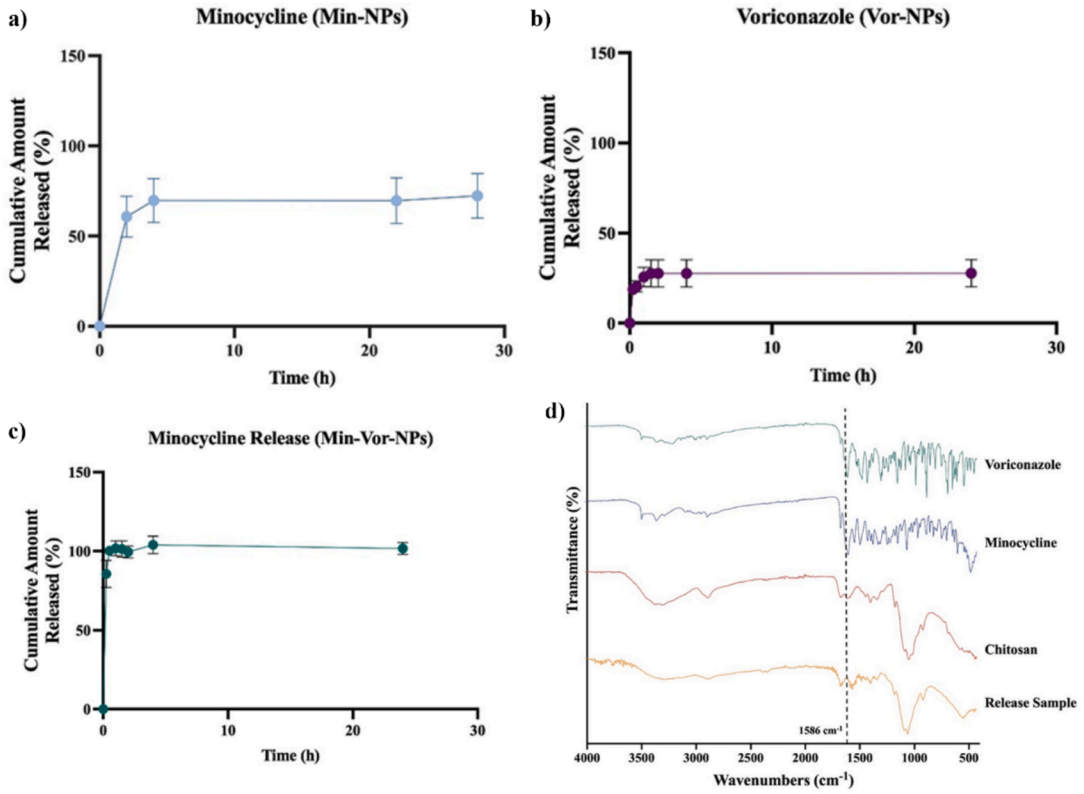

Fig. 2. Experimental *in vitro* cumulative release profile of (a) Min-NPs, (b) Vor-NPs and (c) Min-Vor-NPs. (d) ATR-FTIR of Min-Vor-NPs analyzed after the release assay.

adsorbed drug, and/or polymer degradation (Tao et al., 2021). Swelling usually begins when the polymer encounters the dissolution medium. Thus, the initial burst release of chitosan NPs is probably due to drug diffusion from the polymer surface or holes formed by the swelling. Subsequent polymer degradation and particle erosion can explain the release of the remaining drug. The lower average percent of voriconazole release from Vor-NPs (Fig. 2b) might be due to its hydrophobicity and stronger interaction with the chitosan polymeric matrix (Hubbe, 2019). The dual delivery of drugs may have had a competitor effect on the release profile, as observed in another study (Li et al., 2023).

To confirm the presence of voriconazole in Min-Vor-NPs, ATR-FTIR analysis was performed on the NPs after the release assay. The characteristic peak of voriconazole at 1586 cm^{-1} was identified, as shown in Fig. 2d. As the complexity of drug delivery systems increases, such as with the co-encapsulation of multiple drugs, the thermodynamic challenges of preparing nanoscale materials also grow. When entrapped inside the nanocarriers, drug molecules become spatially close, triggering different interactions such as Van der Waals forces, hydrophobic interactions, and hydrogen bonds formation. Through co-encapsulation, release kinetics may be affected by changes in the biochemistry of the nanomaterial nuclei, such as localized precipitation, disintegration, aggregation, quenching, and intermolecular rearrangements. These transformations are virtually impossible to predict (Bhattacharjee, 2022). Besides, co-encapsulation of drugs into the same nanocarrier might change the drug release profile of the individual drugs (Ingebrigtsen et al., 2017; Renault–Mahieux et al., 2022). Since voriconazole release was restrained in the presence of minocycline, it may be hypothesized that chemical interactions between both drugs and the polymer matrix may lead to changes in drug solubility, preventing its effective release. Of note, strong hydrogen bonding can slow down the drug release by reducing the drug's mobility within the polymer matrix (Singh, 2024). Hence, another possibility is that the co-encapsulation of both drugs modifies the interactions between voriconazole and the chitosan matrix through hydrogen bonding, which magnifies the limited release already observed in the Vor-NPs, preventing the drug release in the Min-Vor-NPs in the observed 24 h.

Noteworthy, minocycline MIC_{50} and MIC_{90} for *S. aureus* are between 0.25 and 8 μg/mL (Trzcinski et al., 2000), respectively. The voriconazole MIC_{90} for *C. albicans* has been established at 0.125 μg/mL (Fothergill et al., 2014). Therefore, these single- and dual-delivery NPs allow to obtain release profiles of minocycline within the therapeutic range. Concerning voriconazole, single-delivery NPs also presented a suitable release profile to target *C. albicans*. The dual-delivery NPs did not achieve the expected release profile for voriconazole, suggesting that further research is needed to improve it. Despite this drawback, the proposed delivery system exhibits undeniable potential for the treatment of osteomyelitis and other polymicrobial infections caused by *S. aureus* or *C. albicans*.

3.4. Antimicrobial activity

As previously stated, biofilm-related infections produced by a monomicrobial species or a combination of bacterial and fungal species have significantly increased, contributing to high levels of morbidity and mortality. Furthermore, polymicrobial biofilms challenge both diagnosis and treatment, requiring complex multi-drug treatment strategies. In general, antimicrobials, primarily broad-spectrum antibiotics, are aimed at a single species within a mixed biofilm (bacteria), allowing non-targeted microorganisms (fungi) to thrive and prolong the infection. As a result, mixed biofilms are an understudied and clinically significant health issue, having the ability to serve as an infectious reservoir for a wide range of microorganisms, including bacteria and fungi (Rodrigues et al., 2019).

This study envisions a strategy to target osteomyelitis where co-infection with *S. aureus* and *C. albicans* is present via a

nanoparticulated co-delivery system (minocycline and voriconazole) based on chitosan and Pluronic® F68. Drug concentrations were defined to accomplish doses above MIC_{50} and MIC_{90} (between 0.25–8 μg/mL) for *S. aureus* and MIC_{90} (0.125 μg/mL) for *C. albicans* (Trzcinski et al., 2000). The microbial density attached to TCP well-plates was quantified after 2- and 24-hour incubation with NPs, and the anti-biofilm activity against mono- and dual-species biofilms was determined.

Regarding mono-species *S. aureus* biofilm, as expected, only the conditions including minocycline showed anti-biofilm activity (Fig. 3). Minocycline (negative control 1) and minocycline-voriconazole mixture (negative control 3) reduced *S. aureus* density by 1.4 Log (96 %) and 1.6 Log (97 %), respectively, after 2 h of incubation (Fig. 3). Voriconazole (negative control 2) did not affect bacterial density compared to positive control 1 (only bacterial biofilm, without NPs or drugs). The b-NPs (positive control 2) and Vor-NPs enabled biofilm formation on the TPC well-plates in the same order of magnitude (c.a 7.4 Log CFUs/mL) as the *S. aureus* solution (positive control 1), showing that empty NPs had no anti-biofilm activity (Fig. 3). Min-NPs and Min-Vor-NPs prevented biofilm formation, lowering *S. aureus* biofilm by 98.9 % (1.89 Log of reduction) and 99 % (2.01 Log of reduction) at 2 h of incubation, respectively. Sessile bacteria density (c.a. 8.5 Log CFUs/mL) significantly increased until 24 h of incubation in the following conditions: *S. aureus* suspension (positive control 1), voriconazole (negative control 2), b-NPs (positive control 2), and Vor-NPs, indicating that these conditions had no anti-biofilm efficacy over time (Fig. 3). A significant drop in sessile bacteria density was observed at 24 h of incubation in the following conditions: minocycline (negative control 1), minocycline-voriconazole mixture (negative control 3), Min-NPs, and Min-Vor-NPs. It should be noted that these bacterial densities were lower than the initial bacterial concentration (6 Log CFUs/mL), indicating that minocycline, minocycline-voriconazole mixture, Min-NPs, and Min-Vor-NPs have bactericidal and anti-biofilm properties (Fig. 3).

Several studies have shown the effectiveness of antibiotics-loaded NPs in targeting *S. aureus*-caused osteomyelitis (Konya et al., 2023; Liu et al., 2022; Min et al., 2016). These studies highlighted the potential of these biomaterials as local antibiotic-delivery systems due to their targeted slow release to the lesion site, replacing systemic antibiotics and reducing the toxic and drugs' side effects. It can also boost local antibiotic concentration, providing more effective bacteriostatic/bactericidal effects, and stimulating bone repair (Konya et al., 2023; Liu et al., 2022; Min et al., 2016).

Mono-species *C. albicans* biofilm was significantly affected by NPs, with and without drugs, and by free voriconazole and minocycline-voriconazole mixture, at 2 h and 24 h of incubation (Fig. 4). At 2 h of incubation, all NPs with and without drugs reduced the *C. albicans* biofilm by 1.2 Log (93 %) compared to positive control 1 (fungal suspension). Free voriconazole (negative control 2) and minocycline-voriconazole mixture (negative control 3) showed anti-fungal activity similar to that of NPs (Fig. 4). As expected, free minocycline (negative control 1) had no antifungal effect. At 24 h of incubation, an increase in fungal density (c.a. 1.3 Log) was observed for all conditions, when compared to sessile *C. albicans* at 2 h. Empty and drug-loaded NPs, and both solutions containing voriconazole, maintained their anti-fungal properties, reducing 1 Log (90 %) the *C. albicans* densities compared to positive control 1 (fungal suspension) (Fig. 4). These data suggest that, besides voriconazole conditions, empty chitosan NPs also have anti-biofilm activity against mono-species *C. albicans* (Fig. 4).

NPs have been described as next-generation anti-fungal agents, due to their properties, like being highly tuneable, with high specific surface area, and physico-chemical features that allow them to attack microorganisms via several different mechanisms. Anti-fungal NPs mechanisms include the release of inorganic ions, membrane damaging, protein, as well as DNA and other critical cellular components, or ROS overproduction, and ATP depletion (Huang et al., 2023).

Although higher voriconazole activity was not detected when encapsulated in NPs in the current work (Fig. 4), probably due to interactions between both antimicrobials within the chitosan matrix, the use of antifungal-loaded NPs could be beneficial in the treatment of fungal osteomyelitis (Huang et al., 2023). These systems may take advantage of the possible synergistic effects of antifungal drugs with NPs, reducing the dosage of both NPs and antifungal drugs as well as reducing the toxicity caused by NPs and antifungal drugs. Besides, the combination of the attacking targets of antifungal drugs and NPs can boost antimicrobial efficacy and the antifungal spectrum and contribute to fight fungal resistance (Huang et al., 2023).

In a dual-species *S. aureus-C. albicans* biofilm, the total number of

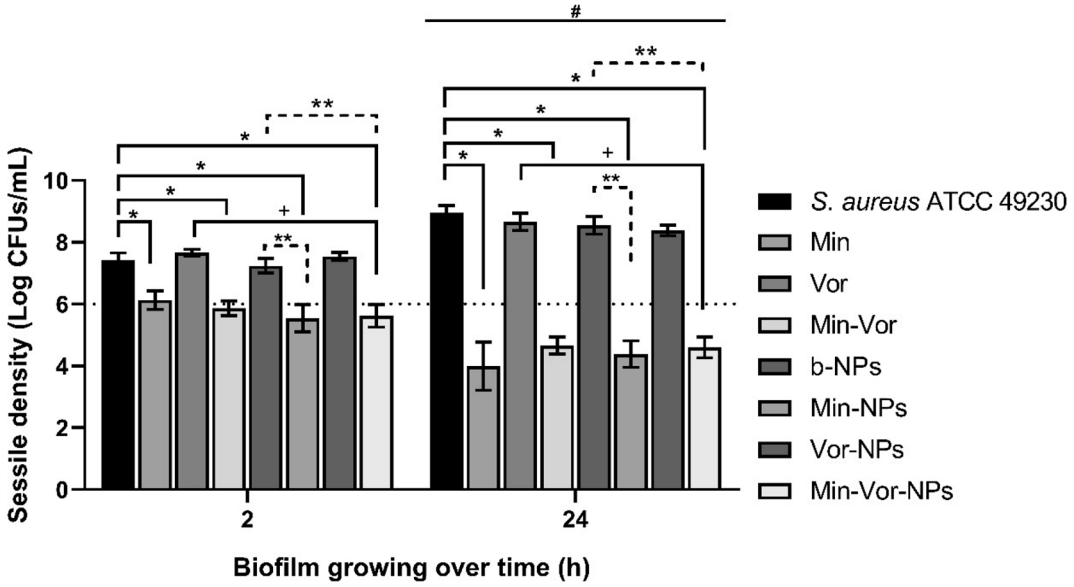

Fig. 3. Anti-biofilm activity of b-NPs, Min-NPs, Vor-NPs, and Min-Vor-NPs against *S. aureus* biofilm. Bacterial densities were expressed in Log CFUs/mL. Positive (b-NPs and *S. aureus* suspension) and negative controls (minocycline, voriconazole, and minocycline-voriconazole solutions) were used to determine the anti-biofilm activity. *Significant differences ($p < 0.05$) between formulations and *S. aureus* suspension (positive control 1). **Significant differences ($p < 0.05$) between drug-loaded NP formulations and b-NPs (positive control 2). $^{+}$Significant differences ($p < 0.05$) between drug-loaded nanoparticle formulations and respective negative controls (minocycline, voriconazole, or minocycline-voriconazole solutions). $^{\#}$Significant differences ($p < 0.05$) between 2 and 24 h for the same condition.

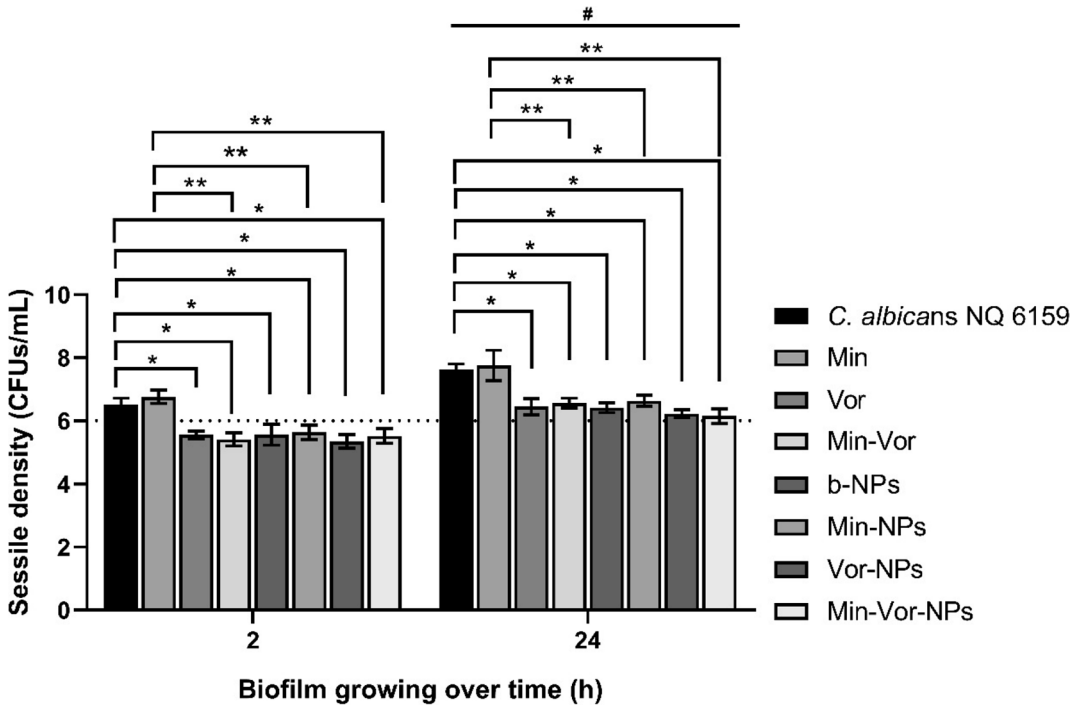

Fig. 4. Anti-biofilm activity of b-NPs, Min-NPs, Vor-NPs, and Min-Vor-NPs against *C. albicans* biofilm. Fungal densities were expressed in Log CFUs/mL. Positive (b-NPs and *C. albicans* suspension) and negative controls (minocycline, voriconazole, and minocycline-voriconazole solutions) were used to determine the anti-biofilm activity. *Significant differences ($p < 0.05$) between formulations and *C. albicans* suspension (positive control 1). **Significant differences ($p < 0.05$) between conditions containing minocycline and minocycline solution (negative control 1). #Significant differences ($p < 0.05$) between 2 and 24 h for the same condition.

sessile cells was significantly affected by Min-NPs, Min-Vor-NPs, and negative controls (minocycline, voriconazole, and minocycline-voriconazole drugs solutions). These formulations reduced by 1.5 Log (97 %) and 3 Log (99.9 %) the biofilm density after 2 and 24 h incubation, respectively (Fig. 5). The b-NPs and Vor-NPs reduced by 1 Log (90 %) of dual-species biofilm when compared to positive control 1 (bacterial and fungal suspension) only after 24 h of incubation (Fig. 5). Looking deep inside the dual-species biofilm, it was found that the presence of Min-NPs and Min-Vor-NPs displayed anti-biofilm activity against *S. aureus*, resulting in a percentage of reduction higher than 95 % over time (Fig. 6). It should be noted that only NPs with minocycline and minocycline-voriconazole had the same anti-biofilm activity as minocycline and minocycline-voriconazole drugs solutions (negative controls 1 and 3, respectively), implying that the antimicrobial action was caused

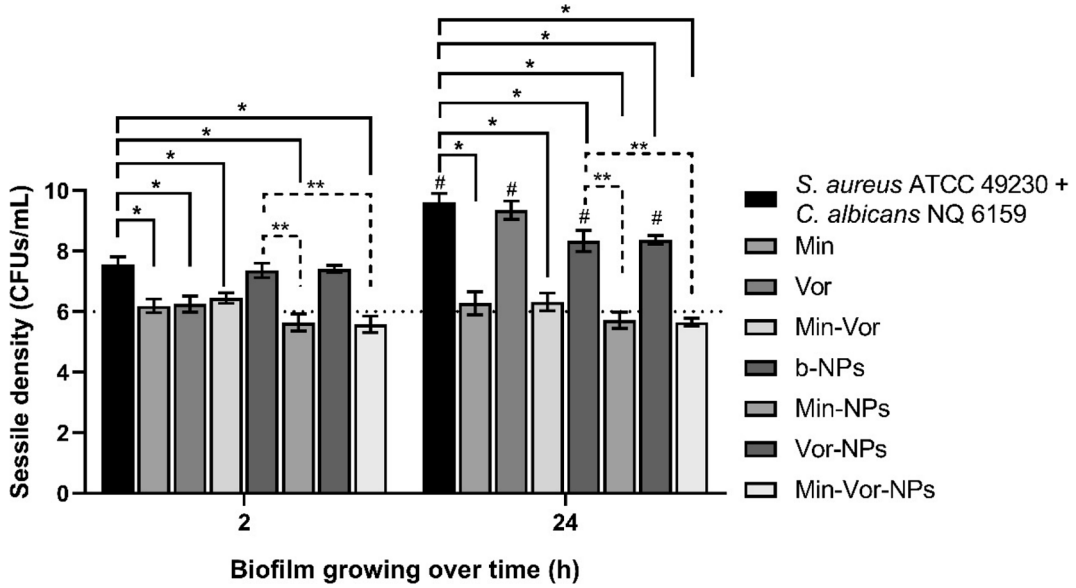

Fig. 5. Anti-biofilm activity of b-NPs, Min-NPs, Vor-NPs, and Min-Vor-NPs against dual-species *S. aureus-C. albicans* biofilm. Dual-species densities were expressed in Log CFUs/mL. Positive (b-NPs and *S. aureus-C. albicans* suspension) and negative controls (minocycline, voriconazole, and minocycline-voriconazole solutions) were used to determine the anti-biofilm activity. *Significant differences ($p < 0.05$) between formulations, and *S. aureus-C. albicans* suspension (positive control 1). **Significant differences ($p < 0.05$) between drug-loaded NP formulations and b-NPs (positive control 2). #Significant differences ($p < 0.05$) between 2 and 24 h for the same condition.

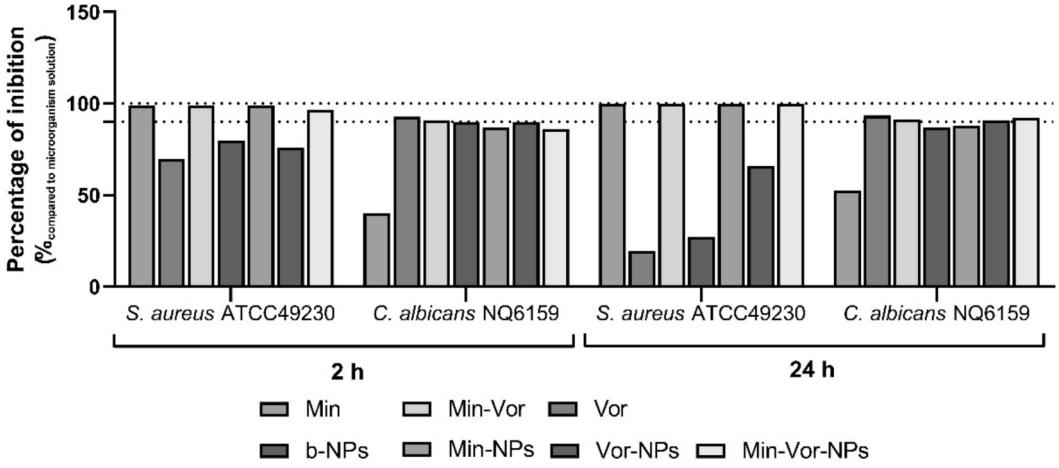

Fig. 6. The percentage of *S. aureus* and *C. albicans* inhibition within a dual-species biofilm. The percentage was calculated by comparing it with the suspension of *S. aureus-C. albicans* (free- NPs and free-antimicrobial agents). TSA plates were used to quantify the total of both *S. aureus* and *C. albicans*, while MSA and SDA plates were used to selectively determine *S. aureus* and *C. albicans* strains, respectively.

by the presence of minocycline in the drug-delivery system (Fig. 6). In the case of *C. albicans* inside dual-species biofilm, a percentual reduction of 90 % of fungi was observed in the presence of NPs, regardless of voriconazole loading (Fig. 6), as previously shown for mono-species *C. albicans* biofilms (Fig. 4). Given the intrinsic antifungal activity of chitosan (Martin et al., 2019), the current data do not allow us to fully isolate voriconazole's contribution to biofilm inhibition.

This study showed that the developed dual-delivery system (minocycline and voriconazole) based on chitosan NPs inhibited biofilm growth but did not entirely eradicate mono- and dual-species biofilms. This could be due to 1) biofilms 3D-structure, which contains a highly resistant microorganism colony wrapped in a self-produced matrix, making eradication significantly more difficult, and 2) the loading concentrations of antimicrobial agents was probably not enough and required to be increased. Nevertheless, this dual-delivery approach reduced the biofilm by more than 90 %, showing promising expectations in the management of biofilm-related infections, such as osteomyelitis.

3.5. Cytocompatibility assays

Multiple functions related to the plasma membrane (transport, respiratory activity, permeability barrier, etc.), can be compromised with the loss of membrane integrity, which may represent significant damage to cells. Impairment of membrane integrity as evaluated by the uptake of membrane-impermeant dyes, is commonly considered an irreversible process (Joux and Lebaron, 2000). The proposed drug-loaded chitosan NPs did not affect cell membrane integrity (Fig. 7) since no significant differences were found in the propidium iodide cellular uptake when compared to the negative control (cells in culture media). As expected, a significant difference was found in the cellular uptake between the negative control (cells in culture media) and the positive control (SDS at 1 mg/mL).

In the MTT assay (Fig. 8), and considering a threshold of 70 % minimum cell viability (Nedeljkovic et al., 2022), there are relevant differences between the two NPs concentrations. In both assays, b-NPs did not show cytotoxicity. Chitosan is clearly described as a non-toxic and biocompatible polymer (Harugade et al., 2023; Pathak et al., 2023). The good cytocompatibility when using osteoblast-like cells was

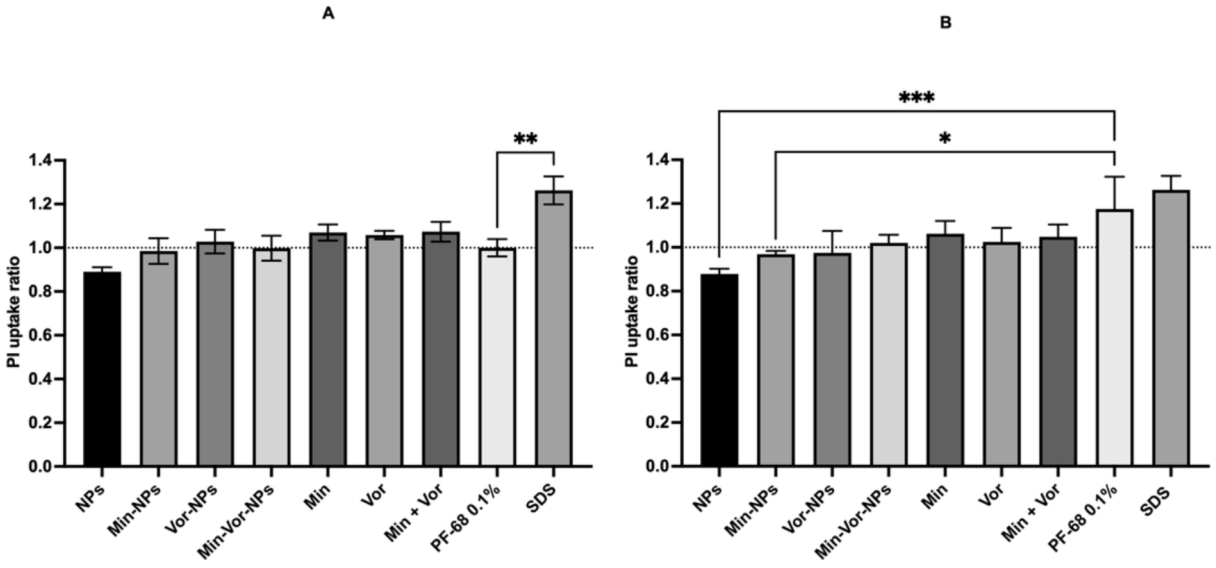

Fig. 7. Membrane integrity of MG-63 cells when cultured with the different groups of NPs (A- 850 μg/mL and B- 425 μg/mL) and with the drugs' solutions for 24 h. No significant differences ($p \leq 0.05$) were found when compared to the medium, used as the negative control. Results are expressed as mean ± SD ($n = 6$).

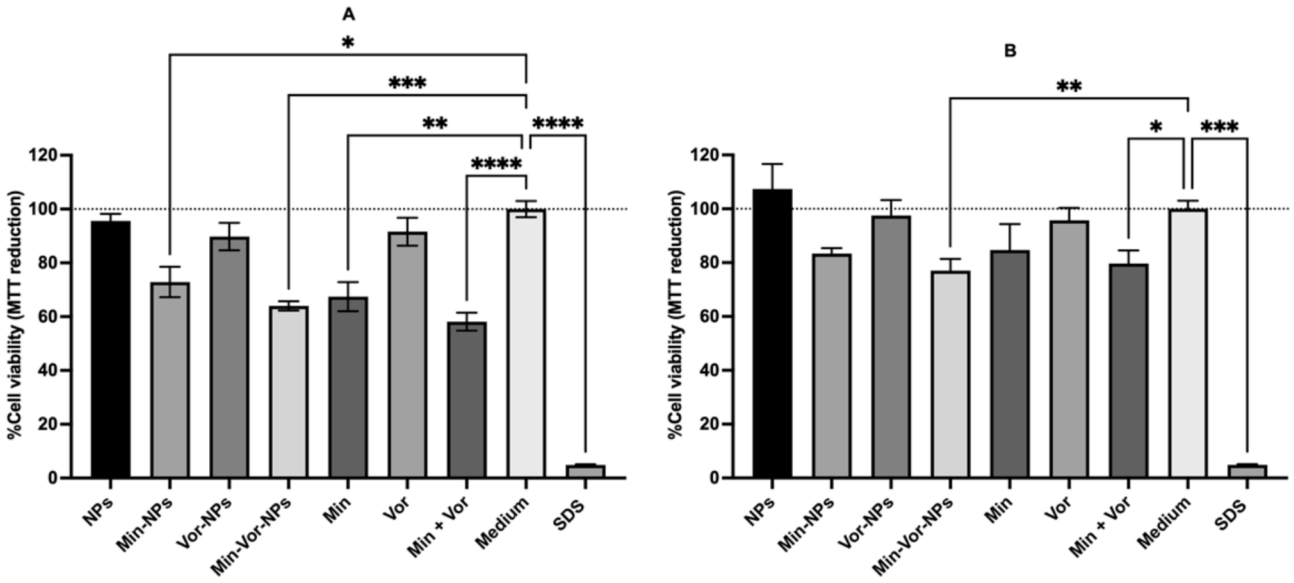

Fig. 8. Metabolic activity (MTT assay) of MG-63 cells when cultured with the different groups of NPs (A- 850 μg/mL and B- 425 μg /mL) and with the drugs' solutions for 24 h. *Significant differences ($p > 0.05$) when compared to the medium, used as positive control, were found. Results are expressed as mean ± SD (n = 6).

an expected outcome.

In assay A (with NPs at 850 μg/mL), cell viability of human osteoblasts significantly decreased with free minocycline and minocycline-voriconazole mixture, but not with free voriconazole. Thus, the observed cytotoxicity can be attributed to minocycline. Min-NPs and Min-Vor-NPs showed a cytotoxic effect, while with Vor-NPs and b-NPs cell viability was near 100 %. These results are in line with previous studies, where the effect of higher levels of minocycline induced a dose-dependent decline of protein expression, cellular differentiation and proliferation in osteoblasts (Almazin et al., 2009) and murine osteoprecursor cells (Park, 2011).

In assay B (with NPs diluted to 425 μg/mL), no cytotoxicity was observed, either with free drugs or the NPs. These results highlight the importance of NPs concentration in biomedical applications, prompting cytotoxicity, directing cell response and viability, as supported by different authors (Peivandi et al., 2024; Xiong et al., 2022).

4. Conclusions

Osteomyelitis is a difficult clinical challenge, especially when a polymicrobial environment is mediated by biofilms. While bacterial osteomyelitis has been extensively characterized, few studies on fungal and mixed osteomyelitis have been carried out. In this study, mono and dual-delivery chitosan-based nanoparticulate systems stabilized with Pluronic® F68 were developed to target bone infections in a polymicrobial environment. Chitosan NPs loaded with single- or dual- antimicrobial agents exhibited *in vitro* cytocompatibility with human osteoblasts, and most importantly, efficacy in reducing polymicrobial biofilms of *S. aureus* and *C. albicans* up to 90 %.

Overall, the findings of this study directly address a critical need in managing osteomyelitis within a polymicrobial ecosystem. The development of NP systems with intrinsic antimicrobial properties, coupled with targeted drug delivery, represents a significant step toward overcoming the limitations of conventional treatments. While we acknowledge that further studies are needed to evaluate the efficacy of voriconazole in this system, our current findings provide compelling evidence of the system's potential. Our work is a substantial step toward addressing the complexities of polymicrobial osteomyelitis treatment.

CRediT authorship contribution statement

M. Zegre: Writing – review & editing, Writing – original draft, Methodology, Investigation, Formal analysis, Data curation, Conceptualization. **J. Barros:** Writing – review & editing, Writing – original draft, Methodology, Investigation, Formal analysis, Data curation, Conceptualization. **A.B. David:** Writing – original draft, Methodology, Investigation, Formal analysis, Data curation. **L. Fialho:** Writing – review & editing, Methodology, Investigation, Formal analysis, Data curation. **M. P. Ferraz:** Writing – review & editing, Supervision, Conceptualization. **FJ. Monteiro:** Writing – review & editing, Supervision, Resources. **L.A. Caetano:** Writing – review & editing, Supervision. **L. Gonçalves:** Writing – review & editing, Validation, Supervision, Methodology, Investigation, Conceptualization. **A. Bettencourt:** Writing – review & editing, Visualization, Validation, Supervision, Resources, Project administration, Funding acquisition, Conceptualization.

Declaration of competing interest

The authors declare that they have no known competing financial interests or personal relationships that could have appeared to influence the work reported in this paper.

Acknowledgments

The authors thank the Fundação para a Ciência e Tecnologia (FCT), Portugal for the financial support of the projects: UIDB/04138/2020 and UIDP/04138/2020 (iMed.Ulisboa); UIDB/05608/2020 and UIDP/05608/2020 (H&TRC). L. Gonçalves, Principal Researcher grant (CEECIND/03143/2017); J. Barros, Junior Researcher Grant (2022.05157.CEECIND/CP1735 /CT0011) and thanks to project Agenda "Health from Portugal - HfPT" [C630926586-00465198], co-financed by the Recovery and Resilience Plan (RRP) and by the European funds NextGeneration EU (https://recuperarportugal.gov.pt/), through the Incentive System "Agendas for Business Innovation"."

The Graphical Abstract was created with Biorender.com.

Data availability

Data will be made available on request.

References

Abinaya, B., Prasith, T.P., Ashwin, B., Viji Chandran, S., Selvamurugan, N., 2019. Chitosan in surface modification for bone tissue engineering applications. Biotechnol. J. 14. https://doi.org/10.1002/biot.201900171.

Agarwal, M., Agarwal, M.K., Shrivastav, N., Pandey, S., Das, R., Gaur, P., 2018. Preparation of Chitosan Nanoparticles and their In-vitro Characterization. Int. J. Life-Sci. Scientif. Res. 4, 1713–1720. https://doi.org/10.21276/ijlssr.2018.4.2.17.

Aibani, N., Rai, R., Patel, P., Cuddihy, G., Wasan, E.K., 2021. Chitosan Nanoparticles at the Biological Interface: Implications for Drug Delivery. Pharmaceutics 13. https://doi.org/10.3390/pharmaceutics13101686.

Almazin, S.M., Dziak, R., Andreana, S., Ciancio, S.G., 2009. The Effect of Doxycycline Hyclate, Chlorhexidine Gluconate, and Minocycline Hydrochloride on Osteoblastic Proliferation and Differentiation In Vitro. J. Periodontol. 80, 999–1005. https://doi.org/10.1902/jop.2009.080574.

Azevedo, M.A., Bourbon, A.I., Vicente, A.A., Cerqueira, M.A., 2014. Alginate/chitosan nanoparticles for encapsulation and controlled release of vitamin B2. Int. J. Biol. Macromol. 71, 141–146. https://doi.org/10.1016/j.ijbiomac.2014.05.036.

Babu, G.S., Raju, C.A.I., 2007. UV-spectrophotometric determination of voriconazole in bulk and its formulation. Asian J. Chem. 19, 1625–1627.

Bettencourt, A.F., Tomé, C., Oliveira, T., Martin, V., Santos, C., Gonçalves, L., Fernandes, M.H., Gomes, P.S., Ribeiro, I.A.C., 2021. Exploring the potential of chitosan-based particles as delivery-carriers for promising antimicrobial glycolipid biosurfactants. Carbohydr. Polym. 254, 117433. https://doi.org/10.1016/j.carbpol.2020.117433.

Bhattacharjee, S., 2022. Craft of Co-encapsulation in Nanomedicine: A Struggle To Achieve Synergy through Reciprocity. ACS Pharmacol. Transl. Sci. 5, 278–298. https://doi.org/10.1021/acsptsci.2c00033.

Bhosale, R., Bhandwalkar, O., Duduskar, A., Jadhav, R., Pawar, P., 2016. Water Soluble Chitosan Mediated Voriconazole Microemulsion as Sustained Carrier for Ophthalmic Application: In vitro/Ex vivo/In vivo Evaluations. Open Pharmaceutical Sciences Journal 3, 215–234. https://doi.org/10.2174/1874844901603010215.

Bury, D.C., Rogers, T.S., Dickman, M.M., 2021. Osteomyelitis: Diagnosis and Treatment. Am. Fam. Physician 104, 395–402.

Chandra Dey, S., Al-Amin, M., Ur Rashid, T., Sultan, Z., Zakir Sultan, M., Ashaduzzaman, M., Sarker, M., Md Shamsuddin, S., 2016. Preparation, characterization and performance evaluation of chitosan as an adsorbent for remazol red. International Journal of Latest Research in Engineering and Technology (IJLRET) Www.ijlret.com 2, 52–62.

de Almeida Campos, L., Fin, M.T., Santos, K.S., de Lima Gualque, M.W., Freire Cabral, A. K.L., Khalil, N.M., Fusco-Almeida, A.M., Mainardes, R.M., Mendes-Giannini, M.J.S., 2023. Nanotechnology-Based Approaches for Voriconazole Delivery Applied to Invasive Fungal Infections. Pharmaceutics 15, 266. https://doi.org/10.3390/pharmaceutics15010266.

Dinarvand, R., Jafarzadeh Kashi, T., Eskandarion, Esfandyari-Manesh, Samadi, Atyabi, F., Eshraghi, 2012. Improved drug loading and antibacterial activity of minocycline-loaded PLGA nanoparticles prepared by solid/oil/water ion pairing method. Int. J. Nanomed. 221. doi: 10.2147/IJN.S27709.

Dinh, P., Hutchinson, B., Zalavras, C., Stevanovic, M., 2009. Reconstruction of Osteomyelitis Defects. Semin. Plast. Surg. 23, 108–118. https://doi.org/10.1055/s-0029-1214163.

El-Hafian, E.A., Elgannoudi, E.S., Mainal, A., Yahaya, A.H.B., 2010. Characterization of chitosan in acetic acid: Rheological and thermal studies. Turk. J. Chem. https://doi.org/10.3906/kim-0901-38.

Enz, A., Mueller, S.C., Warnke, P., Ellenrieder, M., Mittelmeier, W., Klinder, A., 2021. Periprosthetic Fungal Infections in Severe Endoprosthetic Infections of the Hip and Knee Joint—A Retrospective Analysis of a Certified Arthroplasty Centre of Excellence. Journal of Fungi 7, 404. https://doi.org/10.3390/jof7060404.

Fernandes Queiroz, M., Melo, K., Sabry, D., Sassaki, G., Rocha, H., 2014. Does the Use of Chitosan Contribute to Oxalate Kidney Stone Formation? Mar. Drugs 13, 141–158. https://doi.org/10.3390/md13010141.

Fothergill, A.W., Sutton, D.A., McCarthy, D.I., Wiederhold, N.P., 2014. Impact of New Antifungal Breakpoints on Antifungal Resistance in Candida Species. J. Clin. Microbiol. 52, 994–997. https://doi.org/10.1128/JCM.03044-13.

Füredi, P., Pápay, Z.E., Kovács, K., Kiss, B.D., Ludányi, K., Antal, I., Klebovich, I., 2017. Development and characterization of the voriconazole loaded lipid-based nanoparticles. J. Pharm. Biomed. Anal. 132, 184–189. https://doi.org/10.1016/j.jpba.2016.09.047.

Ghosh Dastidar, D., Chakrabarti, G., 2019. Thermoresponsive Drug Delivery Systems, Characterization and Application, in: Applications of Targeted Nano Drugs and Delivery Systems. Elsevier, pp. 133–155. doi: 10.1016/B978-0-12-814029-1.00006-5.

Gimza, B.D., Cassat, J.E., 2021. Mechanisms of Antibiotic Failure During Staphylococcus aureus Osteomyelitis. Front. Immunol. 12. https://doi.org/10.3389/fimmu.2021.638085.

Ha, N.M.C., Nguyen, T.H., Wang, S.-L., Nguyen, A.D., 2019. Preparation of NPK nanofertilizer based on chitosan nanoparticles and its effect on biophysical characteristics and growth of coffee in green house. Res. Chem. Intermed. 45, 51–63. https://doi.org/10.1007/s11164-018-3630-7.

Harugade, A., Sherje, A.P., Pethe, A., 2023. Chitosan: A review on properties, biological activities and recent progress in biomedical applications. React. Funct. Polym. 191, 105634. https://doi.org/10.1016/j.reactfunctpolym.2023.105634.

Holmkvist, A.D., Friberg, A., Nilsson, U.J., Schouenborg, J., 2016. Hydrophobic ion pairing of a minocycline/Ca 2+ /AOT complex for preparation of drug-loaded PLGA nanoparticles with improved sustained release. Int. J. Pharm. 499, 351–357. https://doi.org/10.1016/j.ijpharm.2016.01.011.

Hsu, Y.-H., Yu, Y.-H., Chou, Y.-C., Lu, C.-J., Lin, Y.-T., Ueng, S.-W.-N., Liu, S.-J., 2023. Sustained Release of Antifungal and Antibacterial Agents from Novel Hybrid Degradable Nanofibers for the Treatment of Polymicrobial Osteomyelitis. Int. J. Mol. Sci. 24, 3254. https://doi.org/10.3390/ijms24043254.

Huang, T., Li, X., Maier, M., O'Brien-Simpson, N.M., Heath, D.E., O'Connor, A.J., 2023. Using inorganic nanoparticles to fight fungal infections in the antimicrobial resistant era. Acta Biomater. 158, 56–79. https://doi.org/10.1016/j.actbio.2023.01.019.

Hubbe, M.A., 2019. Why, after all, are chitosan films hydrophobic? BioResources 14, 7630–7631. https://doi.org/10.15376/biores.14.4.7630-7631.

Im, S.-Y., Kim, K.-M., Kwon, J.-S., 2020. Antibacterial and Osteogenic Activity of Titania Nanotubes Modified with Electrospray-Deposited Tetracycline Nanoparticles. Nanomaterials 10, 1093. https://doi.org/10.3390/nano10061093.

Ingebrigtsen, S.G., Škalko-Basnet, N., Jacobsen, C., Holsæter, A.M., 2017. Successful co-encapsulation of benzoyl peroxide and chloramphenicol in liposomes by a novel manufacturing method: dual asymmetric centrifugation. Eur. J. Pharm. Sci. 97, 192–199. https://doi.org/10.1016/j.ejps.2016.11.017.

Jafernik, K., Ładniak, A., Blicharska, E., Czarnek, K., Ekiert, H., Wiącek, A.E., Szopa, A., 2023. Chitosan-Based Nanoparticles as Effective Drug Delivery Systems—A review. Molecules 28, 1963. https://doi.org/10.3390/molecules28041963.

Janakiraman, K., Krishnaswami, V., Sethuraman, V., Natesan, S., Rajendran, V., Kandasamy, R., 2020. Correction to: Development of Methotrexate and Minocycline Loaded Nanoparticles for the Effective Treatment of Rheumatoid Arthritis. AAPS PharmSciTech 21, 92. https://doi.org/10.1208/s12249-020-1634-2.

Joux, F., Lebaron, P., 2000. Use of fluorescent probes to assess physiological functions of bacteriaat single-cell level. Microbes Infect. 2, 1523–1535. https://doi.org/10.1016/S1286-4579(00)01307-1.

Kalepu, S., Nekkanti, V., 2015. Insoluble drug delivery strategies: review of recent advances and business prospects. Acta Pharm. Sin. B 5, 442–453. https://doi.org/10.1016/j.apsb:2015.07.003.

Kamiya, M., Matsumoto, M., Yamashita, K., Izumi, T., Kawaguchi, M., Mizukami, S., Tsurumaru, M., Mukai, H., Kawakami, S., 2022. Stability Study of mRNA-Lipid Nanoparticles Exposed to Various Conditions Based on the Evaluation between Physicochemical Properties and Their Relation with Protein Expression Ability. Pharmaceutics 14, 2357. https://doi.org/10.3390/pharmaceutics14112357.

Karakeçili, A., Topuz, B., Korpayev, S., Erdek, M., 2019. Metal-organic frameworks for on-demand pH controlled delivery of vancomycin from chitosan scaffolds. Mater. Sci. Eng. C 105, 110098. https://doi.org/10.1016/j.msec.2019.110098.

Kim, G.H., Hwang, S.W., Kang, D.H., Jung, B.N., Lee, M.J., Shim, J.K., Seo, K.H., 2020. Controllable synthesis of silica nanoparticle size and packing efficiency onto PVP-functionalized PMMA via a sol–gel method. J. Polym. Sci. 58, 662–672. https://doi.org/10.1002/pol.20190115.

Konya, P., Konya, M.N., Yilmaz, B.K., Kaga, E., Kaga, S., Çetinkol, Y., 2023. Comparison of the Therapeutic Efficacy of Antibiotic-Loaded Polymeric Tissue Scaffold and Bone Cement in the Regeneration of Infected Bone Tissue. Cureus. https://doi.org/10.7759/cureus.46487.

Li, M., Sun, X., Yin, M., Shen, J., Yan, S., 2023. Recent Advances in Nanoparticle-Mediated Co-Delivery System: A Promising Strategy in Medical and Agricultural Field. Int. J. Mol. Sci. 24, 5121. https://doi.org/10.3390/ijms24065121.

Liu, Y., Li, X., Liang, A., 2022. Current research progress of local drug delivery systems based on biodegradable polymers in treating chronic osteomyelitis. Front. Bioeng. Biotechnol. 10. https://doi.org/10.3389/fbioe.2022.1042128.

Liu, Y., Yang, G., Jin, S., Xu, L., Zhao, C., 2020. Development of High-drug-loading Nanoparticles. Chempluschem 85, 2143–2157. https://doi.org/10.1002/cplu.202000496.

Ma, S., Adayi, A., Liu, Z., Li, M., Wu, M., Xiao, L., Sun, Y., Cai, Q., Yang, X., Zhang, X., Gao, P., 2016. Asymmetric Collagen/chitosan Membrane Containing Minocycline-loaded Chitosan Nanoparticles for Guided Bone Regeneration. Sci. Rep. 6, 31822. https://doi.org/10.1038/srep31822.

Martin, V., Francisca Bettencourt, A., Santos, C., Sousa Gomes, P., 2024. Reviewing particulate delivery systems loaded with repurposed tetracyclines – From micro to nanoparticles. Int. J. Pharm. 649, 123642. https://doi.org/10.1016/j.ijpharm.2023.123642.

Martin, V., Ribeiro, I.A.C., Alves, M.M., Gonçalves, L., Almeida, A.J., Grenho, L., Fernandes, M.H., Santos, C.F., Gomes, P.S., Bettencourt, A.F., 2019. Understanding intracellular trafficking and anti-inflammatory effects of minocycline chitosan-nanoparticles in human gingival fibroblasts for periodontal disease treatment. Int. J. Pharm. 572, 118821. https://doi.org/10.1016/j.ijpharm.2019.118821.

Masters, E.A., Ricciardi, B.F., Bentley, K.L.D.M., Moriarty, T.F., Schwarz, E.M., Muthukrishnan, G., 2022. Skeletal infections: microbial pathogenesis, immunity and clinical management. Nat. Rev. Microbiol. 20, 385–400. https://doi.org/10.1038/s41579-022-00686-0.

Matos, A.C., Gonçalves, L.M., Rijo, P., Vaz, M.A., Almeida, A.J., Bettencourt, A.F., 2014. A novel modified acrylic bone cement matrix. A step forward on antibiotic delivery against multiresistant bacteria responsible for prosthetic joint infections. Mater. Sci. Eng. C 38, 218–226. https://doi.org/10.1016/j.msec.2014.02.002.

Mikušová, V., Mikuš, P., 2021. Advances in Chitosan-Based Nanoparticles for Drug Delivery. Int. J. Mol. Sci. 22, 9652. https://doi.org/10.3390/ijms22179652.

Min, J., Choi, K.Y., Dreaden, E.C., Padera, R.F., Braatz, R.D., Spector, M., Hammond, P. T., 2016. Designer Dual Therapy Nanolayered Implant Coatings Eradicate Biofilms and Accelerate Bone Tissue Repair. ACS Nano 10, 4441–4450. https://doi.org/10.1021/acsnano.6b00087.

Miyazawa, T., Itaya, M., Burdeos, G.C., Nakagawa, K., Miyazawa, T., 2021. A Critical Review of the Use of Surfactant-Coated Nanoparticles in Nanomedicine and Food Nanotechnology. Int. J. Nanomed. 16, 3937–3999. https://doi.org/10.2147/IJN.S298606.

Mohan, D., Gupta, V.R.M., 2019. Microsponge based drug delivery system of voriconazole for fungal infection: formulation development and In-vitro evaluation. J. Drug Deliv. Therap. 9, 369–378. https://doi.org/10.22270/jddt.v9i3.2840.

Mohan Raj, R., Duraisamy, N., Raj, V., 2022. Drug loaded chitosan / aloe vera nanocomposite on Ti for orthopedic applications. Mater. Today Proc. 51, 1714–1719. https://doi.org/10.1016/j.matpr.2020.10.772.

Mori, N.M., Patel, P., Sheth, N.R., Rathod, L.V., Ashara, K.C., 2017. Fabrication and characterization of film-forming voriconazole transdermal spray for the treatment of fungal infection. Bull. Fac. Pharm. Cairo Univ. 55, 41–51. https://doi.org/10.1016/j.bfopcu.2017.01.001.

Nagpal, K., Singh, S.K., Mishra, D.N., 2013. Formulation, Optimization, *in Vivo* Pharmacokinetic, Behavioral and Biochemical Estimations of Minocycline Loaded Chitosan Nanoparticles for Enhanced Brain Uptake. Chem. Pharm. Bull. (tokyo) 61, 258–272. https://doi.org/10.1248/cpb.c12-00732.

Nedeljkovic, I., Doulabi, B.Z., Abdelaziz, M., Feilzer, A.J., Exterkate, R.A.M., Szafert, S., Gulia, N., Krejci, I., Kleverlaan, C.J., 2022. Cytotoxicity and anti-biofilm properties of novel hybrid-glass-based caries infiltrant. Dent. Mater. 38, 2052–2061. https://doi.org/10.1016/j.dental.2022.11.018.

Park, J.-B., 2011. Effects of Doxycycline, Minocycline, and Tetracycline on Cell Proliferation, Differentiation, and Protein Expression in Osteoprecursor Cells. Journal of Craniofacial Surgery 22, 1839–1842. https://doi.org/10.1097/SCS.0b013e31822e8216.

Pathak, R., Bhatt, S., Punetha, V.D., Punetha, M., 2023. Chitosan nanoparticles and based composites as a biocompatible vehicle for drug delivery: A review. Int. J. Biol. Macromol. 253, 127369. https://doi.org/10.1016/j.ijbiomac.2023.127369.

Peivandi, Z., Shirazi, F.H., Teimourian, S., Farnam, G., Babaei, V., Mehrparvar, N., Koohsari, N., Ashtarinezhad, A., 2024. Silica nanoparticles-induced cytotoxicity and genotoxicity in A549 cell lines. Sci. Rep. 14, 14484. https://doi.org/10.1038/s41598-024-65333-5.

Phan, H.T., Haes, A.J., 2019. What Does Nanoparticle Stability Mean? J. Phys. Chem. C 123, 16495–16507. https://doi.org/10.1021/acs.jpcc.9b00913.

Rabima, R., Sari, M.P., 2019. Entrapment efficiency and drug loading of curcumin nanostructured lipid carrier (NLC) formula. Pharmaciana 9, 299. https://doi.org/10.12928/pharmaciana.v9i2.13070.

Rasyid, N.Q., Sugita, P., Ambarsari, L., Syahbirin, G., 2014. Suspension Stability and Characterization of Chitosan Nanoparticle–Coated Ketoprofen Based on Surfactants Oleic Acid and Poloxamer 188. Makara J Sci 18. https://doi.org/10.7454/mss.v18i3.3720.

Reddy, M., Tejaswi, Y., Kalyan, A.V., Sravya, R., Namrath, M., 2014. Novel drug delivery of Minocycline aganist bacteria by using a polymer citric acid macro molecule. Indian J. Res. Pharm. Biotechnol. 2, 1161–1166.

Rodrigues, M.E., Gomes, F., Rodrigues, C.F., 2019. Candida spp./Bacteria Mixed Biofilms. Journal of Fungi 6, 5. https://doi.org/10.3390/jof6010005.

Rodrigues, M.A., Tiago, J.M., Padrela, L., Matos, H.A., Nunes, T.G., Pinheiro, L., Almeida, A.J., de Azevedo, E.G., 2014. New Thermoresistant Polymorph from CO2 Recrystallization of Minocycline Hydrochloride. Pharm. Res. 31, 3136–3149. https://doi.org/10.1007/s11095-014-1406-3.

Sarmento, B., Ferreira, D., Veiga, F., Ribeiro, A., 2006. Characterization of insulin-loaded alginate nanoparticles produced by ionotropic pre-gelation through DSC and FTIR studies. Carbohydr. Polym. 66, 1–7. https://doi.org/10.1016/j.carbpol.2006.02.008.

Schmidt, B.M., Keeney-Bonthrone, T.P., Hawes, A.M., Karmakar, M., Frydrych, L.M., Cinti, S.K., Pop-Busui, R., Delano, M.J., 2023. Comorbid status in patients with osteomyelitis is associated with long-term incidence of extremity amputation. BMJ Open Diabetes Res. Care 11, e003611. https://doi.org/10.1136/bmjdrc-2023-003611.

Shah, M.K.A., Azad, A.K., Nawaz, A., Ullah, S., Latif, M.S., Rahman, H., Alsharif, K.F., Alzahrani, K.J., El-Kott, A.F., Albrakati, A., Abdel-Daim, M.M., 2021. Formulation Development, Characterization and Antifungal Evaluation of Chitosan NPs for Topical Delivery of Voriconazole In Vitro and Ex Vivo. Polymers (basel) 14, 135. https://doi.org/10.3390/polym14010135.

Shi, S., Shi, W., Zhou, B., Qiu, S., 2024. Research and Application of Chitosan Nanoparticles in Orthopedic Infections. Int. J. Nanomed. 19, 6589–6602. https://doi.org/10.2147/IJN.S468848.

Siddiqui, A., Jain, P., Alex, T.S., Ali, M.A., Hassan, N., Haneef, J., Naseef, P.P., Kuruniyan, M.S., Mirza, M.A., Iqbal, Z., 2022. Investigation of a minocycline-loaded nanoemulgel for the treatment of acne rosacea. Pharmaceutics 14 (11), 2322. https://doi.org/10.3390/pharmaceutics14112322.

Silva, T., Grenho, L., Barros, J., Silva, J.C., Pinto, R.V., Matos, A., Colaço, B., Fernandes, M.H., Bettencourt, A., Gomes, P.S., 2017. A minocycline-releasing PMMA system as a space maintainer for staged bone reconstructions— *in vitro* antibacterial, cytocompatibility and anti-inflammatory characterization. Biomed. Mater. 12, 035009. https://doi.org/10.1088/1748-605X/aa68b8.

Simpson, E., Sarwar, H., Jack, I., Lowry, D., 2024. Evaluation of the Potential of Chitosan Nanoparticles as a Delivery Vehicle for Gentamicin for the Treatment of Osteomyelitis. Antibiotics 13, 208. https://doi.org/10.3390/antibiotics13030208.

Singh, D., 2024. A Pioneer Review on Intermolecular Hydrogen Bonding in Drug-Polymer Mixtures: Implication of a Stable Delivery System. J. Macromol. Sci. Part B 1–17. https://doi.org/10.1080/00222348.2024.2397918.

Tao, F., Ma, S., Tao, H., Jin, L., Luo, Y., Zheng, J., Xiang, W., Deng, H., 2021. Chitosan-based drug delivery systems: From synthesis strategy to osteomyelitis treatment – A review. Carbohydr. Polym. 251, 117063. https://doi.org/10.1016/j.carbpol.2020.117063.

Tao, J., Zhang, Y., Shen, A., Yang, Y., Diao, L., Wang, L., Cai, D., Hu, Y., 2020. Injectable Chitosan-Based Thermosensitive Hydrogel/Nanoparticle-Loaded System for Local Delivery of Vancomycin in the Treatment of Osteomyelitis . Int. J. Nanomed. 15, 5855–5871. https://doi.org/10.2147/IJN.S247088.

Trzcinski, K., Cooper, B.S., Hryniewicz, W., Dowson, C.G., 2000. Expression of resistance to tetracyclines in strains of methicillin-resistant Staphylococcus aureus. J. Antimicrob. Chemother. 45, 763–770. https://doi.org/10.1093/jac/45.6.763.

Üstündağ Okur, N., Çağlar, E.Ş., Yozgatli, V., 2016. Development and validation of an HPLC method for voriconazole active substance in bulk and its pharmaceutical formulation. Marmara Pharm. J. 20, 79. https://doi.org/10.12991/mpj.20162076793.

Warsito, M.F., Agustiani, F., 2021. A review on factors affecting chitosan nanoparticles formation. IOP Conf. Ser.: Mater. Sci. Eng. 1011, 012027. https://doi.org/10.1088/1757-899X/1011/1/012027.

Wen, C., Xu, X., Zhang, Y., Xia, J., Liang, Y., Xu, L., 2024. Bone Targeting Nanoparticles for the Treatment of Osteoporosis. Int. J. Nanomed. 19, 1363–1383. https://doi.org/10.2147/IJN.S444347.

Xiong, P., Huang, X., Ye, N., Lu, Q., Zhang, G., Peng, S., Wang, H., Liu, Y., 2022. Cytotoxicity of Metal-Based Nanoparticles: From Mechanisms and Methods of Evaluation to Pathological Manifestations. Adv. Sci. 9. https://doi.org/10.1002/advs.202106049.

Yanat, M., Schroën, K., 2021. Preparation methods and applications of chitosan nanoparticles; with an outlook toward reinforcement of biodegradable packaging. React. Funct. Polym. 161, 104849. https://doi.org/10.1016/j.reactfunctpolym.2021.104849.

Yazdanbakhsh, A., Behzadi, A., Moghaddam, A., Salahshoori, I., Khonakdar, H.A., 2023. Mechanisms and factors affecting the removal of minocycline from aqueous solutions using graphene-modified resorcinol formaldehyde aerogels. Sci. Rep. 13, 22771. https://doi.org/10.1038/s41598-023-50125-0.

Zapata, D., Higgs, J., Wittholt, H., Chittimalli, K., Brooks, A.E., Mulinti, P., 2022. Nanotechnology in the Diagnosis and Treatment of Osteomyelitis. Pharmaceutics. https://doi.org/10.3390/pharmaceutics14081563.

Zbinovsky, V., Chrekian, G.P., 1977. Minocycline. pp. 323–339. doi: 10.1016/S0099-5428(08)60348-2.

Zegre, M., Barros, J., Ribeiro, I.A.C., Santos, C., Caetano, L.A., Gonçalves, L., Monteiro, F. J., Ferraz, M.P., Bettencourt, A., 2022. Poly(DL-lactic acid) scaffolds as a bone targeting platform for the co-delivery of antimicrobial agents against S. aureus-C. albicans mixed biofilms. Int. J. Pharm. 622, 121832. https://doi.org/10.1016/j.ijpharm.2022.121832.